



Cite this: *Dalton Trans.*, 2022, **51**, 12569Received 23rd May 2022,  
Accepted 29th July 2022DOI: 10.1039/d2dt01606k  
rsc.li/dalton

# Selective photocatalytic CO<sub>2</sub> reduction by cobalt dicyanamide†

Sina Sadigh Akbari <sup>a</sup> and Ferdi Karadas <sup>\*a,b</sup>

Photocatalytic conversion of CO<sub>2</sub> into chemical fuels is a promising approach to tackle carbon emission and global warming. Herein, we promote a cobalt dicyanamide coordination compound, **Co-dca**, for the first time, as a selective catalyst to reduce CO<sub>2</sub> to CO in the presence of a ruthenium photosensitizer (Ru PS) under visible light irradiation. **Co-dca** was prepared by a facile precipitation method and characterized by Infrared, UV-Vis, XRD, SEM, TEM, and XPS studies. A series of photocatalytic experiments under various reaction conditions were performed to reveal the role of the PS, the scavenger, and the solvent in the selectivity and the activity of the photocatalytic process. We find that **Co-dca** exhibits an activity of 254 μmol h<sup>-1</sup> g<sup>-1</sup> and a CO selectivity as high as 93%.

## Introduction

The production of fuels from CO<sub>2</sub> in the atmosphere is a promising yet challenging approach for clean energy conversion and storage.<sup>1,2</sup> The critical challenges in the CO<sub>2</sub> reduction reaction (CO<sub>2</sub>RR) involve sluggish kinetics and low selectivity.<sup>3–6</sup> Among the various catalytic methods, an unbiased photocatalytic reduction of CO<sub>2</sub> to yield valuable chemicals such as CO, formate, methane, and methanol has attracted attention.<sup>7–10</sup>

The photocatalytic CO<sub>2</sub> reduction performances of new catalytic assemblies have been commonly probed with a [Ru(bpy)<sub>3</sub>]<sup>2+</sup> (bpy = 2,2'-bipyridine) photosensitizer/a sacrificial electron donor pair.<sup>4</sup> Phthalocyanines,<sup>11,12</sup> MOFs,<sup>13–16</sup> oxides,<sup>17,18</sup> LDHs,<sup>19,20</sup> and most recently Prussian blue analogues (PBAs) have been utilized as heterogeneous catalysts for photocatalytic conversion of CO<sub>2</sub> to CO.<sup>21</sup> Particularly, the studies on metal phthalocyanines reveal that capping ligands, which allow partial delocalization, play a critical role in the catalytic activity and selectivity of the CO<sub>2</sub> to CO conversion process.<sup>22–25</sup>

Dicyanamide (dca), [N(CN)<sub>2</sub>]<sup>-</sup>, is an N-donor bridging group, which forms polymeric compounds with transition metals by using its nitrogen atoms for coordination. It is considered a pseudo-halide as it displays chemical and coordination properties similar to group 17 anions.<sup>26</sup> Furthermore, a

relatively short dicyanamide bridging ligand allows magnetic and electronic communication between metal ions. This communication also provides partial electron transfer between neighboring metal ions, utilized for electrocatalytic and magnetic studies.<sup>27–29</sup>

Given the partial electron delocalization and the proper coordination environment of cobalt ions in cobalt dicyanamide, we utilize a dicyanamide-based coordination polymer for photocatalytic CO<sub>2</sub> reduction for the first time. The photocatalytic activity of a 3D coordination compound, Co(dca)<sub>2</sub>, was investigated in the presence of [Ru(bpy)<sub>3</sub>]<sup>2+</sup> as the light-harvesting component and TEOA as the electron donor sacrificial agent.

## Experimental section

### Preparation of Co-dca

Typically, an aqueous solution (4 mL) of NaN(CN)<sub>2</sub> (9 mmol, Acros Organics, 97%) was added dropwise to a solution containing Co(NO<sub>3</sub>)<sub>2</sub>·6H<sub>2</sub>O (4 mL, 4.5 mmol, Alfa Aesar, 99.9%) at room temperature. After 4 h stirring, the resulting light-pink precipitate was collected by centrifugation, rinsed thoroughly with water, and finally dried at 75 °C.

### Photocatalytic CO<sub>2</sub> reduction experiment

The photocatalytic experiments were carried out in a 16.5 mL Pyrex reactor at room temperature. Typically, 10 mg catalyst, 3.74 mg [Ru(bpy)<sub>3</sub>]Cl<sub>2</sub>·6H<sub>2</sub>O (0.5 mM, Sigma-Aldrich, 99.95%), 8 mL acetonitrile (MeCN, Sigma-Aldrich, >99.9%), and 2 mL triethanolamine (TEOA, as the sacrificial agent, Acros Organics, 97%) were added in the reactor. The reaction solution was purged with CO<sub>2</sub> gas for 30 min before light

<sup>a</sup>Department of Chemistry, Faculty of Science, Bilkent University, 06800 Ankara, Turkey. E-mail: karadas@fen.bilkent.edu.tr

<sup>b</sup>UNAM – National Nanotechnology Research Center, Institute of Materials Science and Nanotechnology, Bilkent University, 06800 Ankara, Turkey

† Electronic supplementary information (ESI) available. See DOI: <https://doi.org/10.1039/d2dt01606k>

irradiation. A Xe lamp (300 W; AM 1.5 global filter) equipped with a UV filter ( $\lambda > 420$  nm) was used as a light source. The amount of generated gas was determined by injecting 100  $\mu\text{L}$  of the reactor headspace gas into a gas chromatograph (Agilent 7820A GC) equipped with a Molesieve column and a TCD detector.

### Characterization

Fourier transform infrared (FT-IR) spectra were recorded with a Bruker Alpha Platinum-ATR spectrometer. Analyses were performed in the transmission mode and in a wavenumber range between 400 and 4000  $\text{cm}^{-1}$  with a resolution of 4  $\text{cm}^{-1}$ . Powder X-ray diffraction (XRD) patterns of samples were obtained on a Pananalytical X'PertPro multipurpose X-ray diffractometer (MPD) using Cu  $K_{\alpha}$  X-ray radiation ( $\lambda = 1.5418$  Å) with a scan step of 0.04 within the range of 10–70°. X-ray Photoelectron (XPS) measurements were performed with a Thermo Scientific K-Alpha X-ray photoelectron spectrometer system equipped with an Al  $K_{\alpha}$  micro-focused monochromator source (1486.6 eV) operating at 400  $\mu\text{m}$  spot size and accompanied by a flood gun for charge neutralization. The morphology and chemical composition of the samples were characterized by a scanning electron microscope (SEM, FEI-Quanta 200 FEG ESEM), associated with an energy dispersive X-ray spectrometer (EDS) analyzer. Transmission electron microscopy (TEM) examinations were carried out at 300 kV using an FEI Technai G2 F30 transmission electron microscope. UV-Vis absorption spectra were recorded on the Cary 5000 UV-A-Vis-NIR spectrometer equipped with a Varian Cary 2500 internal diffuse reflectance (DR) accessory.

## Results and discussion

Cobalt dicyanamide, **Co-dca**, was prepared by a straightforward precipitation method.<sup>30</sup> Each cobalt site is coordinated to six  $[\text{N}(\text{CN})_2]^-$  ligands *via* the four nitrile nitrogens and two central amido nitrogens. The octahedral cobalt sites are slightly elongated, in which the two axial amido nitrogens are located slightly farther from the metal center than the four equatorial nitrile nitrogens.<sup>31</sup> Cobalt sites on the surface, thus, exhibit coordination environments similar to those in CoFe Prussian blue analogues and cobalt phthalocyanines since they are surrounded by a combination of water molecules and nitrogen atoms of the dicyanamide groups.<sup>32</sup>

The structure of **Co-dca** is elucidated with Fourier transform infrared (FTIR) spectroscopy and powder X-ray diffraction (XRD). The FTIR spectrum of **Co-dca** reveals absorption bands in the 2030–2420  $\text{cm}^{-1}$  range, which correspond to the asymmetric and symmetric stretches of  $\nu(\text{C}\equiv\text{N})$ . Two bands are also observed at 963  $\text{cm}^{-1}$  and 1314  $\text{cm}^{-1}$ , which can be assigned to  $\nu_{\text{s}}(\text{N}-\text{C})$  and  $\nu_{\text{as}}(\text{N}-\text{C})$ , respectively (Fig. 1a and Table S1†).<sup>27,33,34</sup> The obtained experimental powder XRD pattern is identical to a previously reported  $\text{Co}(\text{dca})_2$  crystal structure (CCDC 117729†), in which octahedral cobalt sites are surrounded by dicyanamide ligands to form a 3D coordination network (Fig. 1b). Dicyanamide ligand uses both its nitrile ( $-\text{CN}$ ) and amide ( $\text{NC}-\text{N}-\text{CN}$ ) nitrogen atoms for coordination (Fig. S1†).<sup>27,30</sup>

The morphology and structure of the sample were studied by scanning electron microscopy (SEM) and transmission electron microscopy (TEM) analyses. SEM and TEM images reveal

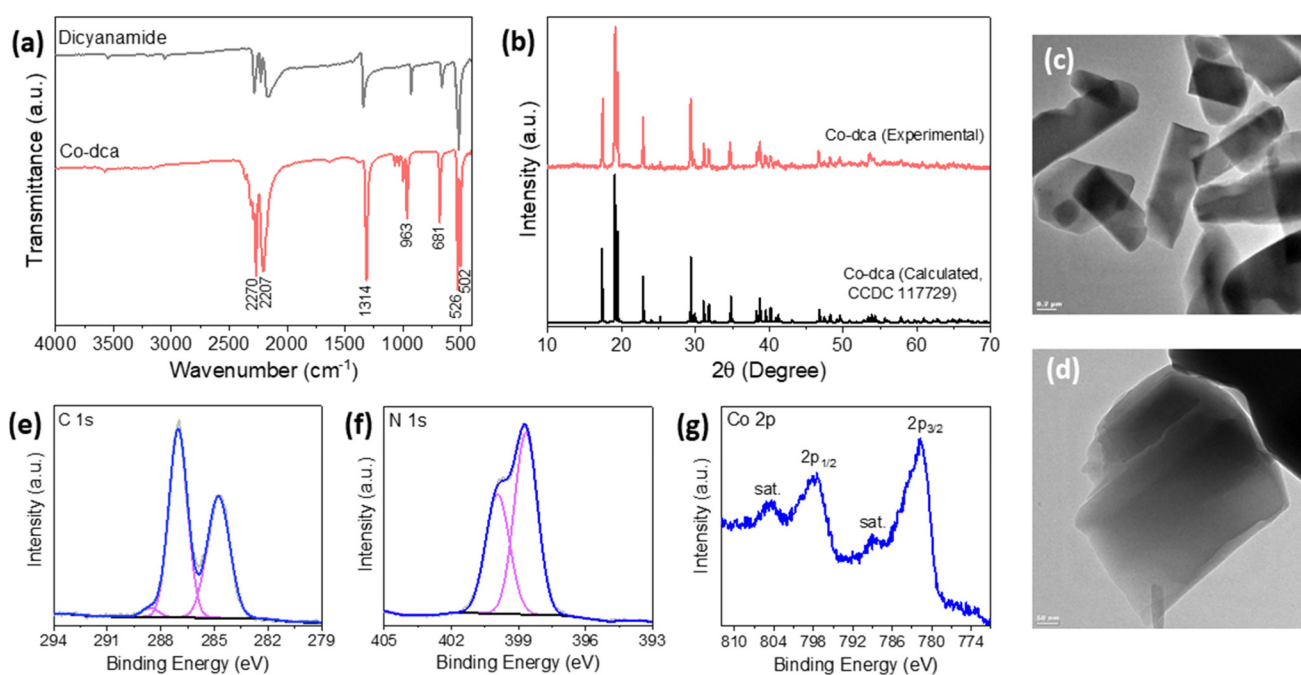


**Fig. 1** (a) ATR-FTIR spectra of **Co-dca** sample and  $\text{NaN}(\text{CN})_2$ . (b) Experimental and calculated (CCDC 117729†) XRD patterns of **Co-dca**. (c and d) TEM images of **Co-dca**. XPS spectra of (e) C 1s, (f) N 1s, and (g) Co 2p for pristine **Co-dca**.

that the **Co-dca** is constructed with cubic brick subunits with a micrometer size (Fig. 1c, d and S2†). The chemical composition of **Co-dca** was determined by energy-dispersive X-ray spectroscopy (EDS), and the Co:C:N elemental ratio was found to be 7.7:38.7:52.1, which is in agreement with the stoichiometric ratio of **Co-dca** (Fig. S3 and S4†).

An X-ray photoelectron spectroscopy (XPS) analysis was carried out to investigate the chemical composition of the **Co-dca**. In the C 1s spectrum, the three peaks at 284.8, 287.1 and 288.6 eV correspond to C–C, carbon bonded to N in the dicyanamide (N–C≡N), and the surface C=O bond, respectively (Fig. 1e).<sup>35,36</sup> The N 1s region is deconvoluted to two peaks at 398.7 and 399.9 eV, which are assigned to the nitrile nitrogen and the central amido nitrogen in the dicyanamide structure, respectively (Fig. 1f).<sup>37,38</sup> The Co 2p spectrum exhibits two broad peaks at 781.8 and 797.9 eV, ascribed to Co 2p<sub>3/2</sub> and Co 2p<sub>1/2</sub>, respectively. Another doublet at slightly higher binding energies can be attributed to shake-up satellite peaks (Fig. 1g). Previous studies reveal that the Co 2p<sub>3/2</sub>–Co 2p<sub>1/2</sub> spin-orbit splitting is 15 eV for diamagnetic Co(III) complexes and 16 eV for paramagnetic Co(II) complexes.<sup>39</sup> Moreover, cobalt(II) complexes show broader 2p<sub>3/2</sub> and 2p<sub>1/2</sub> lines with more intense satellite peaks than cobalt(III) complexes.<sup>40,41</sup> The presence of satellite peaks, broad 2p<sub>3/2</sub> and 2p<sub>1/2</sub> lines,

and spin-orbit splitting of 16.1 eV suggests that cobalt cations are mainly in their +2 oxidation states in **Co-dca**.<sup>40,42</sup>

The photocatalytic activity of **Co-dca** was evaluated in the presence of a ruthenium photosensitizer (Ru PS), [Ru(bpy)<sub>3</sub>]Cl<sub>2</sub>·6H<sub>2</sub>O (bpy = 2′2′-bipyridine), and an electron donor, triethanolamine (TEOA), under visible light irradiation. A series of control experiments were performed to determine the role of each component in the photocatalytic CO<sub>2</sub> reduction process (Fig. 2a and b). In the presence of the photosensitizer and catalyst, CO<sub>2</sub> was reduced into CO with a rate of 2.54 μmol h<sup>-1</sup> and H<sub>2</sub> with a rate of 0.7 μmol h<sup>-1</sup>, which yields a selectivity of 79% (entry 1). The complete inhibition of the activity without a Ru photosensitizer or without light irradiation (dark condition) proves that the CO<sub>2</sub> reduction process involves the excitation of the photosensitizer by the absorption of light (entries 2 and 3). When the catalyst, **Co-dca**, is not present, the amount of produced CO is reduced drastically from 2.54 μmol h<sup>-1</sup> to 0.37 μmol h<sup>-1</sup> and an approximately three-fold increase is observed in the amount of evolved H<sub>2</sub>. In other words, hydrogen evolution reaction (HER) dominates over CO<sub>2</sub>RR when **Co-dca** is absent, indicating the critical role of **Co-dca** as the catalyst in selective photocatalytic CO<sub>2</sub>RR (entry 4). To examine the effect of dicyanamide ligand on the catalytic activity of [Ru(bpy)<sub>3</sub>]<sup>2+</sup>, bare dca was employed in the photo-

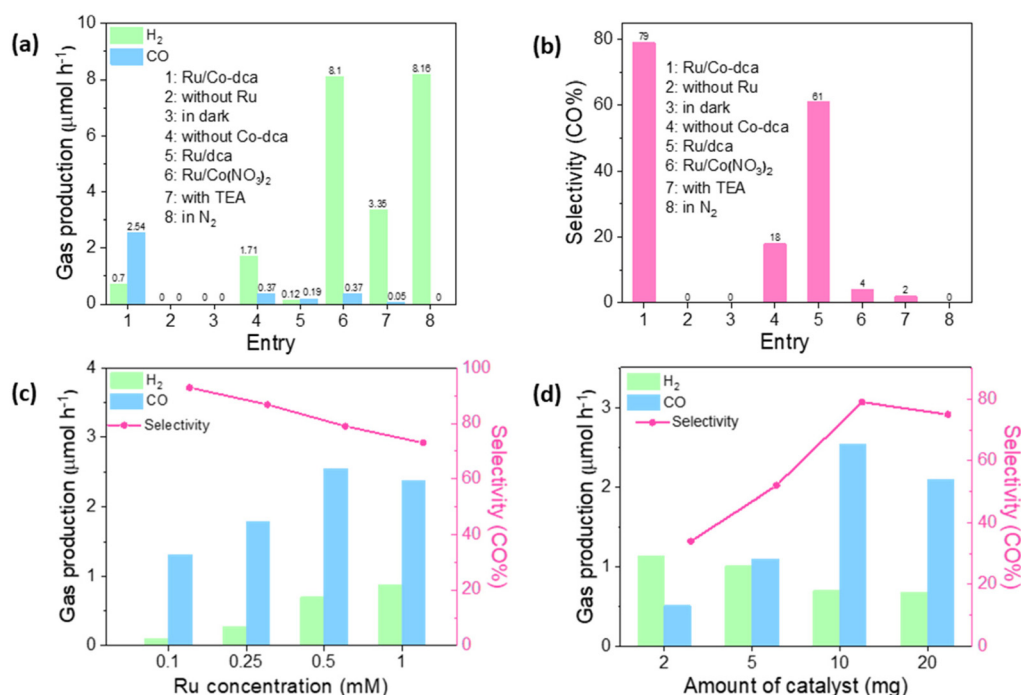


**Fig. 2** (a) Rates of CO and H<sub>2</sub> evolution, and (b) corresponding selectivity of photocatalytic CO<sub>2</sub> to CO conversion over H<sub>2</sub> evolution. The reactions are performed with **Co-dca**, [Ru(bpy)<sub>3</sub>]<sup>2+</sup>, and TEOA (entry 1), without [Ru(bpy)<sub>3</sub>]<sup>2+</sup> (entry 2), without light (entry 3), without **Co-dca** (entry 4), when bare dca ligand is used as the catalyst (entry 5), when **Co-dca** is replaced with Co(NO<sub>3</sub>)<sub>2</sub> as the catalyst (entry 6), when TEOA is replaced with TEA (entry 7), and when the measurement is performed under N<sub>2</sub> atmosphere in place of CO<sub>2</sub> (entry 8). Regular reaction conditions: 10 mg catalyst, 3.74 mg [Ru(bpy)<sub>3</sub>]Cl<sub>2</sub>·6H<sub>2</sub>O (0.5 mM), 8 mL acetonitrile, and 2 mL TEOA at 25 °C, 30 min purging with CO<sub>2</sub> under visible light irradiation (λ > 420 nm). (c) The effect of the concentration of [Ru(bpy)<sub>3</sub>]Cl<sub>2</sub> on the evolution of CO, H<sub>2</sub>, and the selectivity of CO over H<sub>2</sub> under photocatalytic conditions. (d) The effect of the quantity of **Co-dca** on the evolution of CO, H<sub>2</sub>, and the selectivity of CO over H<sub>2</sub> under photocatalytic conditions.

catalytic CO<sub>2</sub> reduction (entry 5). The total production of CO and H<sub>2</sub> was significantly decreased, which reveals that the interaction between dca and decomposed Ru photosensitizer does not lead to an active catalyst for CO<sub>2</sub>RR and HER. Co(NO<sub>3</sub>)<sub>2</sub> was also replaced with **Co-dca** to elucidate the effect of dca groups on the catalytic activity (entry 6). When Co(NO<sub>3</sub>)<sub>2</sub> is used as the catalyst, a similar CO production rate is obtained to the “without catalyst” case, entry 2, while HER activity increases up to around 8.1 μmol h<sup>-1</sup>. The dramatic difference in the selectivity indicates that a cobalt site surrounded with nitrogen atoms of dca ligand is selective towards CO<sub>2</sub>RR while the dominant process is HER when a bare cobalt ion is surrounded with oxygen atoms.<sup>43,44</sup> Our photocatalytic experiments also confirm that CO<sub>2</sub>-to-CO conversion is not observed when TEOA is replaced with triethylamine (TEA; entry 7). Under N<sub>2</sub> atmosphere, no generation of CO was observed, confirming that CO is derived exclusively from CO<sub>2</sub>, as expected (entry 8).

We further studied the effect of the concentration of Ru PS on photocatalytic performance (Fig. 2c). The H<sub>2</sub> evolution rate increases with increasing the concentration of the Ru PS. The activity of CO<sub>2</sub>RR reaches a maximum in the presence of a 0.5 mM Ru PS. However, the selectivity for CO<sub>2</sub>-to-CO conversion is gradually reduced with increasing the amount of Ru photosensitizer, and the highest selectivity is obtained when 0.1 mM Ru is used (93%).

When the amount of catalyst is varied, CO<sub>2</sub>RR activity reaches a maximum value of 254 μmol g<sup>-1</sup> h<sup>-1</sup> when 10 mg catalyst is used (Fig. 2d). In contrast, the H<sub>2</sub> production rate is gradually reduced with increasing the amount of catalyst, revealing that **Co-dca** is more selective towards CO<sub>2</sub> reduction than H<sub>2</sub> evolution. The selectivity profiles in Fig. 2c and d, thus, suggest that catalytic HER mainly occurs on the ruthenium sites, which are produced by the decomposition of molecular [Ru(bpy)<sub>3</sub>]<sup>2+</sup> complexes during photoexcitation.<sup>4,45,46</sup> Studies on the reaction time reveal a linear relationship between the amount of CO and the irradiation time during the 1<sup>st</sup> hour of the photocatalytic process. The activity is, however, gradually lost and the CO production rate significantly decreases during the 2<sup>nd</sup> cycle (Fig. S5†).

The catalytic activity of **Co-dca** was compared with CoFe Prussian blue, CoFe-PB, which has recently been studied for the photocatalytic CO<sub>2</sub>RR in the presence of Ru PS. The maximum activity for CoFe-PB was obtained when the concentration of the Ru PS was 1 mM. **Co-dca** exhibits a CO generation activity of 2.38 μmol h<sup>-1</sup> in the 1<sup>st</sup> hour, which is ca. 3.5 times higher than that of CoFe-PB (Fig. S6a†). The higher selectivity of CO<sub>2</sub>RR obtained for **Co-dca** compared to CoFe-PB reveals that cobalt is more selective towards CO<sub>2</sub>RR when it is surrounded with dicyanamide groups compared to cyanide groups (Fig. S6b†).

Previous studies on CO<sub>2</sub>RR report that water should be used for photocatalytic CO<sub>2</sub> reduction.<sup>4</sup> Our results, however, demonstrate that **Co-dca** exhibits a higher performance in the absence of water (Fig. S7†). **Co-dca** was dispersed in various

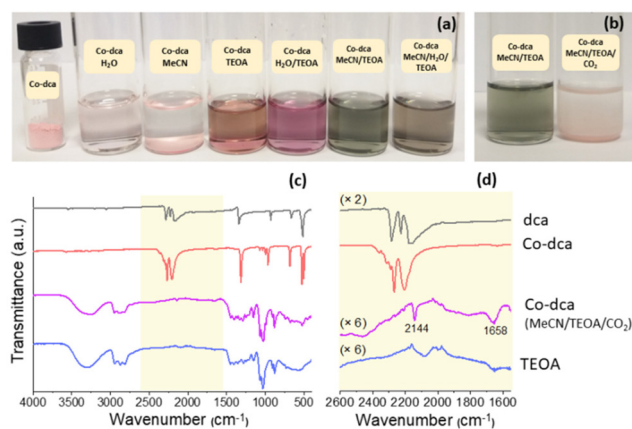


**Fig. 3** (a) **Co-dca** powder dispersed in different solutions. (b) **Co-dca** powder dispersed in MeCN/TEOA solution with and without CO<sub>2</sub> bubbling. ATR-FTIR spectra of dca, **Co-dca**, **Co-dca** in MeCN/TEOA/CO<sub>2</sub> solution, and TEOA between (c) 400–4000 cm<sup>-1</sup>, and (d) 1550–2600 cm<sup>-1</sup>.

solvents to understand the effect of the solvent molecules on the structure of the catalyst (Fig. 3a). **Co-dca** exhibits a pink color in H<sub>2</sub>O and MeCN similar to its color in the powder form, a red color in TEOA and H<sub>2</sub>O/TEOA, and a dark green color in MeCN/TEOA and MeCN/H<sub>2</sub>O/TEOA solutions. The UV-Vis absorption spectra of **Co-dca** in H<sub>2</sub>O and MeCN/TEOA solutions were investigated (Fig. S8†). The clear color change and different absorption profile in TEOA could be attributed to the coordination of TEOA molecules to accessible cobalt sites. Note that **Co-dca** is not soluble in MeCN. When the transparent solution of **Co-dca** in MeCN/TEOA solution is bubbled with CO<sub>2</sub> and stirred for 2 h, the dark greenish color turns to a cloud due to the formation of a precipitate (Fig. 3b). Infrared studies performed on this precipitate reveal that the coordination environment of cobalt sites is altered slightly as cyanide stretch modes shift to lower wavenumbers compared to pristine **Co-dca** powder (Fig. 3c). Previous studies indicate that TEOA serves not only as a scavenger but also participates actively in the catalytic mechanism by binding to the catalytic metal center to assist the activation of CO<sub>2</sub> molecules.<sup>47,48</sup> The color change with the addition of TEOA could, thus, be attributed to the coordination of TEOA to the cobalt sites and the formation of a precipitate after purging with CO<sub>2</sub> is due to the binding of TEOA groups to the CO<sub>2</sub> molecule. The C=O stretching vibration at 1658 cm<sup>-1</sup> is observed for **Co-dca** in MeCN/TEOA/CO<sub>2</sub>, which supports the assumption that TEOA may react with CO<sub>2</sub> (Fig. 3d).<sup>49</sup>

The chemical structure of the post-catalytic sample was investigated with FTIR, XPS, UV-Vis absorption, and TEM techniques. The post-catalytic **Co-dca** sample exhibits CN bands similar to the **Co-dca** in MeCN/TEOA/CO<sub>2</sub> solution (Fig. 3d), suggesting that the dicyanamide is still retained in the structure after the photocatalytic experiment. The additional bands in the spectrum can be attributed to TEOA (Fig. 4a). Moreover, the post-catalytic sample exhibits the C=O stretching vibration



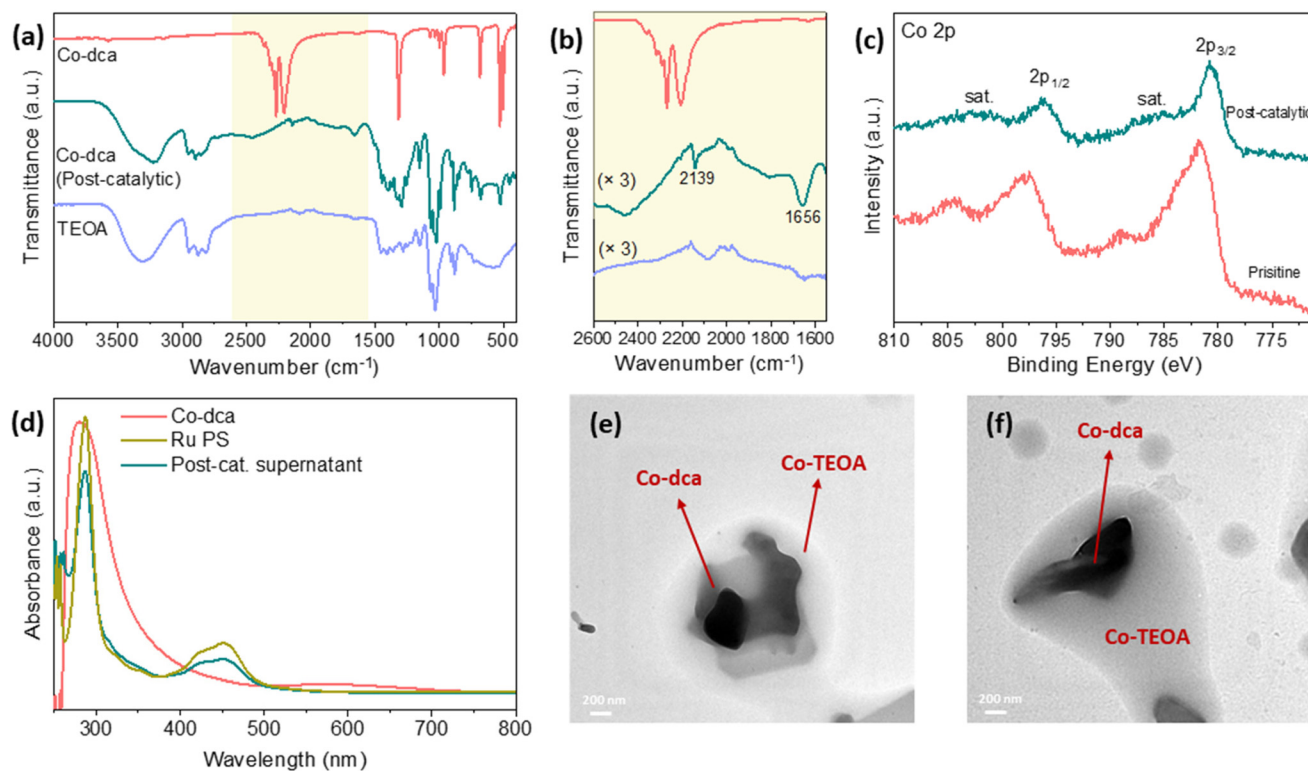


**Fig. 4** ATR-FTIR spectra of **Co-dca**, post-catalytic **Co-dca**, and TEOA between (a) 400–4000  $\text{cm}^{-1}$ , and (b) 1550–2600  $\text{cm}^{-1}$ . (c) XPS Co 2p spectra of pristine and post-catalytic **Co-dca**. (d) UV-Vis absorption spectra of **Co-dca** (10 mg),  $[\text{Ru}(\text{bpy})_3]\text{Cl}_2$  (0.5 mM), and supernatant solution of the post-catalytic sample. (All spectra were recorded in a solution containing 8 mL acetonitrile and 2 mL TEOA.) (e and f) TEM images of **Co-dca** for post-catalytic sample.

at 1656  $\text{cm}^{-1}$  (Fig. 4b). Co 2 $p_{3/2}$  and 2 $p_{1/2}$  peaks get narrower, and the spin–orbit splitting ( $\Delta E = 15.6$  eV) is reduced slightly compared to the pristine **Co-dca**, which indicates that  $\text{Co}^{2+}$  ions are partially oxidized to  $\text{Co}^{3+}$  during the photocatalytic process, as proposed for cobalt-based  $\text{CO}_2\text{RR}$  (Fig. 4c).<sup>50</sup> The UV-Vis absorption spectra of **Co-dca** and  $[\text{Ru}(\text{bpy})_3]^{2+}$  in acetonitrile/TEOA (8 mL/2 mL) solution and the supernatant solution of the post-catalytic sample are demonstrated in Fig. 4d for comparison.  $[\text{Ru}(\text{bpy})_3]^{2+}$  displays a characteristic absorption at 453 nm attributed to the metal to ligand charge transfer (MLCT), along with a sharp band at 287 nm.<sup>51</sup> The UV-Vis absorption profile for the post-catalytic supernatant solution is essentially the same as  $[\text{Ru}(\text{bpy})_3]^{2+}$ , suggesting that **Co-dca** forms a precipitate during the photocatalytic process. TEM images and EDS analysis reveal that **Co-dca** particles have been coated with slightly thick **Co-TEOA** layers, which could form by leaching of cobalt ions to coordinate to TEOA from multiple sites (Fig. 4e, f and S9†).<sup>52–54</sup> The decrease in the activity of **Co-dca** in the 2<sup>nd</sup> cycle could, thus, be attributed to the transformation of active cobalt sites to inactive **Co-TEOA** layers. Furthermore, the TEOA coordinated cobalt cations are significantly active for  $\text{H}_2$  evolution reaction,<sup>43,44</sup> which could be the reason for the higher  $\text{H}_2$  production selectivity of the photocatalytic system in the 2<sup>nd</sup> cycle (Fig. S10†). Overall, we suggest that TEOA coordinates to cobalt sites, which are active towards

the  $\text{CO}_2\text{RR}$  process. TEOA binds further to cobalt sites during the photocatalytic process to produce **Co-TEOA** particles, which are inactive towards  $\text{CO}_2\text{RR}$ .

## Conclusion

In summary, a cobalt dicyanamide coordination compound, **Co-dca**, was successfully synthesized *via* a straightforward precipitation method. Characterization studies reveal that the compound exhibits an extended network structure, in which the cobalt sites are surrounded with the nitrogen atoms of the dicyanamide ligands. Photocatalytic studies indicate that **Co-dca** exhibits a  $\text{CO}_2$ -to-CO conversion rate of 254  $\mu\text{mol h}^{-1} \text{g}^{-1}$  (0.5 mM Ru PS) and a selectivity of as high as 93% CO (0.1 mM Ru PS). We also observed that the CO production activity of **Co-dca** is *ca.* 3.5 times higher than that of CoFe-PB, which has recently been investigated for photocatalytic  $\text{CO}_2\text{RR}$ . Characterization studies on the post-catalytic sample reveal the formation of the **Co-TEOA** particles, which are inactive towards  $\text{CO}_2\text{RR}$ .

## Conflicts of interest

There are no conflicts to declare.

## Acknowledgements

This work is supported by the Scientific and Technological Research Council of Turkey (TUBITAK), grant number 121Z227. S. S. A. thanks TUBITAK for support (Project No: 119C219).

## Notes and references

- 1 Y. Zheng, J. Qiao, J. Yuan, J. Shen, A.-j. Wang, P. Gong, X. Weng and L. Niu, *Electrochim. Acta*, 2018, **282**, 735–742.
- 2 H. J. Son, C. Pac and S. O. Kang, *Acc. Chem. Res.*, 2021, **54**, 4530–4544.
- 3 J. Wu, Y. Huang, W. Ye and Y. Li, *Adv. Sci.*, 2017, **4**, 1–29.
- 4 Y. Yamazaki, H. Takeda and O. Ishitani, *J. Photochem. Photobiol., C*, 2015, **25**, 106–137.
- 5 E. Fujita, *Coord. Chem. Rev.*, 1999, **185–186**, 373–384.
- 6 H. Takeda and O. Ishitani, *Coord. Chem. Rev.*, 2010, **254**, 346–354.
- 7 A. Nakada, H. Kumagai, M. Robert, O. Ishitani and K. Maeda, *Acc. Mater. Res.*, 2021, **2**, 458–470.
- 8 Y. Tamaki and O. Ishitani, *ACS Catal.*, 2017, **7**, 3394–3409.
- 9 H. Chen, L. Chen, G. Chen, M. Robert and T. C. Lau, *ChemPhysChem*, 2021, **22**, 1835–1843.
- 10 J. Di, B. Lin, B. Tang, S. Guo, J. Zhou and Z. Liu, *Small Struct.*, 2021, **2**, 2100046.
- 11 J. Grodkowski, T. Dhanasekaran, P. Neta, P. Hambright, B. S. Brunschwig, K. Shinozaki and E. Fujita, *J. Phys. Chem. A*, 2000, **104**, 11332–11339.
- 12 S. Roy and E. Reisner, *Angew. Chem., Int. Ed.*, 2019, **58**, 12180–12184.
- 13 S. Wang, W. Yao, J. Lin, Z. Ding and X. Wang, *Angew. Chem., Int. Ed.*, 2014, **53**, 1034–1038.
- 14 Z. Y. Du, Y. Z. Yu, N. F. Li, Y. S. Xue, L. X. Xu, H. Mei and Y. Xu, *Sustainable Energy Fuels*, 2021, **5**, 3876–3883.
- 15 X. Deng, Y. Qin, M. Hao and Z. Li, *Inorg. Chem.*, 2019, **58**, 16574–16580.
- 16 X. K. Wang, J. Liu, L. Zhang, L. Z. Dong, S. L. Li, Y. H. Kan, D. S. Li and Y. Q. Lan, *ACS Catal.*, 2019, **9**, 1726–1732.
- 17 S. Wang, Y. Hou and X. Wang, *ACS Appl. Mater. Interfaces*, 2015, **7**, 4327–4335.
- 18 C. Gao, Q. Meng, K. Zhao, H. Yin, D. Wang, J. Guo, S. Zhao, L. Chang, M. He, Q. Li, H. Zhao, X. Huang, Y. Gao and Z. Tang, *Adv. Mater.*, 2016, **28**, 6485–6490.
- 19 S. Bai, Z. Wang, L. Tan, G. I. N. Waterhouse, Y. Zhao and Y. F. Song, *Ind. Eng. Chem. Res.*, 2020, **59**, 5848–5857.
- 20 L. Tan, S. Xu, Z. Wang, Y. Xu, X. Wang, X. Hao, S. Bai, C. Ning, Y. Wang, W. Zhang, Y. K. Jo, S. Hwang, X. Cao, X. Zheng, H. Yan, Y. Zhao, H. Duan and Y. Song, *Angew. Chem., Int. Ed.*, 2019, **58**, 11860–11867.
- 21 X. Meng, J. Yang, C. Zhang, Y. Fu, K. Li, M. Sun, X. Wang, C. Dong, B. Ma and Y. Ding, *ACS Catal.*, 2022, **12**, 89–100.
- 22 Y. Liu and C. C. L. McCrory, *Nat. Commun.*, 2019, **10**, 1–10.
- 23 T. Abe, H. Imai, T. Yoshida, S. Tokita, D. Schlettwein, D. Wöhrle and M. Kaneko, *J. Porphyrins Phthalocyanines*, 1997, **01**, 315–321.
- 24 S. Meshitsuka, M. Ichikawa and K. Tamaru, *J. Chem. Soc., Chem. Commun.*, 1974, 158–159.
- 25 T. Abe, T. Yoshida, S. Tokita, F. Taguchi, H. Imai and M. Kaneko, *J. Electroanal. Chem.*, 1996, **412**, 125–132.
- 26 D. R. Turner, A. S. R. Chesman, K. S. Murray, G. B. Deacon and S. R. Batten, *Chem. Commun.*, 2011, **47**, 10189–10210.
- 27 M. Kurmoo and C. J. Kepert, *New J. Chem.*, 1998, **22**, 1515–1524.
- 28 S. R. Batten and K. S. Murray, *Coord. Chem. Rev.*, 2003, **246**, 103–130.
- 29 A. Tekin, O. Karalti and F. Karadas, *Microporous Mesoporous Mater.*, 2016, **228**, 153–157.
- 30 J. L. Manson, C. R. Kmety, Q. Z. Huang, J. W. Lynn, G. M. Bendele, S. Pagola, P. W. Stephens, L. M. Liable-Sands, A. L. Rheingold, A. J. Epstein and J. S. Miller, *Chem. Mater.*, 1998, **10**, 2552–2560.
- 31 S. R. Batten, P. Jensen, B. Moubaraki, K. S. Murray and R. Robson, *Chem. Commun.*, 1998, **3**, 439–440.
- 32 T. G. Ulusoy Ghobadi, E. Ozbay and F. Karadas, *Chem. – Eur. J.*, 2021, **27**, 3638–3649.
- 33 J. Palion-Gazda, K. Choroba, B. Machura, A. Świtlicka, R. Kruszynski, J. Cano, F. Lloret and M. Julve, *Dalton Trans.*, 2019, **48**, 17266–17280.
- 34 M. Mann, O. Reckeweg, N. Nöthling, R. Goddard and R. Dronskowski, *Inorganics*, 2018, **6**, 135.
- 35 A. Sivanantham, P. Ganesan, L. Estevez, B. P. McGrail, R. K. Motkuri and S. Shanmugam, *Adv. Energy Mater.*, 2018, **8**, 1702838.
- 36 N. Hellgren, R. T. Haasch, S. Schmidt, L. Hultman and I. Petrov, *Carbon*, 2016, **108**, 242–252.
- 37 J. K. Chang, M. T. Lee, W. T. Tsai, M. J. Deng and I. W. Sun, *Chem. Mater.*, 2009, **21**, 2688–2695.
- 38 H. Hashimoto, A. Ohno, K. Nakajima, M. Suzuki, H. Tsuji and K. Kimura, *Surf. Sci.*, 2010, **604**, 464–469.
- 39 T. Ivanova, A. Naumkin, A. Sidorov, I. Eremenko and M. Kiskin, *J. Electron Spectrosc. Relat. Phenom.*, 2007, **156–158**, 200–203.
- 40 H. Haraguchi, K. Fujiwara and F. Keiichiro, *Chem. Lett.*, 1975, **4**, 409–414.
- 41 D. Briggs and V. A. Gibson, *Chem. Phys. Lett.*, 1974, **25**, 493–496.
- 42 G. S. Stucky, T. A. Carlson and G. A. Vernon, *Inorg. Chem.*, 1976, **15**, 278–284.
- 43 J. Dong, M. Wang, X. Li, L. Chen, Y. He and L. Sun, *ChemSusChem*, 2012, **5**, 2133–2138.
- 44 J. Wang, K. Feng, B. Chen, Z. J. Li, Q. Y. Meng, L. P. Zhang, C. H. Tung and L. Z. Wu, *J. Photochem. Photobiol., A*, 2016, **331**, 247–254.
- 45 G. H. Allen, R. P. White, D. P. Rillema and T. J. Meyer, *J. Am. Chem. Soc.*, 1984, **106**, 2613–2620.
- 46 B. Durham, J. V. Caspar, J. K. Nagle and T. J. Meyer, *J. Am. Chem. Soc.*, 1982, **104**, 4803–4810.

- 47 T. Morimoto, T. Nakajima, S. Sawa, R. Nakanishi, D. Imori and O. Ishitani, *J. Am. Chem. Soc.*, 2013, **135**, 16825–16828.
- 48 H. Koizumi, H. Chiba, A. Sugihara, M. Iwamura, K. Nozaki and O. Ishitani, *Chem. Sci.*, 2019, **10**, 3080–3088.
- 49 R. N. Sampaio, D. C. Grills, D. E. Polyansky, D. J. Szalda and E. Fujita, *J. Am. Chem. Soc.*, 2020, **142**, 2413–2428.
- 50 E. Boutin, L. Merakeb, B. Ma, B. Boudy, M. Wang, J. Bonin, E. Anxolabéhère-Mallart and M. Robert, *Chem. Soc. Rev.*, 2020, **49**, 5772–5809.
- 51 N. H. Damrauer, G. Cerullo, A. Yeh, T. R. Bousie, C. V. Shank and J. K. McCusker, *Science*, 1997, **275**, 54–57.
- 52 K. J. Rutt and M. N. Hughes, *J. Chem. Soc. A*, 1968, 2788–2790.
- 53 Y. Kuge and S. Yamada, *Bull. Chem. Soc. Jpn.*, 1969, **42**, 2552–2555.
- 54 S. R. Hosseinian, V. Tangoulis, M. Menelaou, C. P. Raptopoulou, V. Psycharis and C. Dendrinou-Samara, *Dalton Trans.*, 2013, **42**, 5355–5366.